 CMES, vol.38, no.1, pp.59-87, 2008

A Method Based on Wavelets for Band Structure Analysis of Phononic Crystals

Zhi-Zhong Yan[1,2], Yue-Sheng Wang[1,3] and Chuanzeng Zhang[2]

Abstract: In this paper, a numerical method based on the wavelet theory is developed for calculating band structures of 2D phononic crystals consisting of general anisotropic materials. After systematical consideration of the appropriate choice of wavelets, two types of wavelets, the Haar wavelet and Biorthogonal wavelet, are selected. Combined with the supercell technique, the developed method can be then applied to compute the band structures of phononic crystals with point or line defects. We illustrate the advantages of the method both mathematically and numerically. Particularly some representative numerical examples are presented for various material combinations (solid-solid, solid-fluid and fluid-fluid) with complex lattice structures to show the accuracy, fast convergence and wide applicability of the method.

Keywords: elastic wave, phononic crystal, band structure, wavelet, numerical method

1 Introduction

The phononic crystal (also termed the acoustic band gap material) is a composite medium composed of periodic arrays of two or more materials with different mass densities and elastic properties. In analogy to photonic crystals (Joannopoulos et al. 1995), phononic crystals may exhibit complete (or absolute) band gaps in their transmission spectra where the propagation of acoustic or elastic waves is strictly forbidden in all directions (if not in all directions, then we have directional band gaps). The complete band gaps could be engineered to provide a vibration-less environment for high precision mechanical systems in given frequency ranges. Understanding the full band structures (including both stop-bands and pass-bands) is expected to lead to the design of new generations of sound shields, filters, trans-

[1] Institute of Engineering Mechanics, Beijing Jiaotong University, Beijing 100044, China
[2] Department of Civil Engineering, University of Siegen, D-57068 Siegen, Germany
[3] Corresponding author. Tel: +86-10-51688417, E-mail:yswang@bjtu.edu.cn

ducers, refractive devices such as acoustic lenses and acoustic interferometers, etc. By breaking the periodicity of the systems, it is possible to create highly localized defect or guided modes within the acoustic band gaps, which are analogous to localized modes in a photonic crystal (Bayindir et al. 2000) and to localized impurity states in a semiconductor (Yablonovitch et al. 1991). This makes the phononic crystals potential candidates for the design of elastic or acoustic wave guides. Because of these promising applications, the propagation of elastic or acoustic waves in phononic crystals has received increasing attention in the past decade. Here, we would not exhaust all literatures but refer to the homepage http://www.phys.uoa.gr/phononics for a comprehensive list of references on this topic.

Although much progress has been made on photonic crystals, phononic crystals should deserve more attentions because of their rich physics as well as the characteristics of the mixed longitudinal and transverse waves with different velocities which distinguish them from photonic crystals. However, in comparing with the photonic crystals, we know less about phononic crystals and are still far away from practical applications.

A typical case of a phononic crystal in two-dimension is composed of a periodic array (in *x*-*y* plane) of material *A* embedded in a background material *B*. Both materials *A* and *B* are general anisotropic media (solids, liquid or gas). In this inhomogeneous linearly elastic anisotropic system with no body force, the motion equation of harmonic plane waves for the displacement vector $\mathbf{u}(\mathbf{r})$ can be written as

$$-\rho(\mathbf{r})\omega^2\mathbf{u}(\mathbf{r}) = \nabla\cdot(\mathbb{C}(\mathbf{r}):\nabla\mathbf{u}(\mathbf{r})) \tag{1.1}$$

where $\mathbf{r}=(x,y)$ is the position vector; ω is the circular frequency; $\nabla=(\frac{\partial}{\partial x},\frac{\partial}{\partial y})$ is the two-dimensional nabla; ":" denotes the double contraction; $\rho(\mathbf{r})$ and $\mathbb{C}(\mathbf{r})$ are the position-dependent mass density and elastic stiffness tensor, respectively. For isotropic systems, the elements of $\mathbb{C}(r)$ are $C_{ijkl}=\lambda(\mathbf{r})\delta_{ij}\delta_{kl}+\mu(\mathbf{r})(\delta_{ik}\delta_{jl}+\delta_{il}\delta_{jk})$ where $\lambda(\mathbf{r})$ is the Lamé constant and $\mu(\mathbf{r})$ the shear modulus; and for fluids, we can simply set $\mu(\mathbf{r})\equiv 0$. One basic task in research about phononic crystals is to compute the band structures of the periodic problem (1.1).

Two main strategies are usually employed in computing Eq. (1.1). One consists of band structure calculations of the corresponding infinite system. The other calculates the transmission spectra by different algorithms. In the first strategy, the plane wave expansion (PWE) method is one of the commonly used methods (for a review on this method see Kushwaha 1999). However, this method has several drawbacks. First, the elastic parameters, $\rho(\mathbf{r})$ and $\mathbb{C}(\mathbf{r})$, are discontinuous. In PWE method, these discontinuous step functions are reconstructed from a series of

continuous sine and cosine functions. Since a uniformly convergent series of continuous functions always yields a continuous function, the Fourier series of the discontinuous elastic functions cannot be uniformly convergent. Although the Fourier series yields convergence of the mean, the series overshoots the actual values at the simple discontinuities. This is known as the Gibbs phenomenon. As the number of the expansion terms is increased, the overshoots and undershoots increase while moving closer to the discontinuity and the elastic functions can even become negative. On the other hand, when the number of the expansion terms is small, there are large spatial fluctuations and possible local negative values of the elastic functions. Another difficulty with PWE method is that the matrices appearing therein are usually full. This makes the algorithms computationally expensive and thus significantly limits the number of wave modes that can be taken into account. Furthermore, in some situations the PWE method may gives unphysical flat frequency bands and may be unable to give accurate results for the mixed solid/fluid systems (Goffaux and Vigneron 2001). In the second strategy, the often used methods include multiple scattering theory (MST) method (Kafesaki and Economou 1999; Sainidou et al. 2004; Li et al. 2006) and finite difference time domain (FDTD) method (Sigalas and Garcia 2000; Wang et al. 2003; Hsieh et al. 2006), etc. The MST method based on the well-known Korringa-Kohn-Rostoke theory is a useful method to deal with the 3D cases including the mixed solid/fluid systems and those with a large contrast in properties of the component materials, but is much complex in computation and also requires a large number of terms in the multiple expansion. The FDTD method is mainly used in finite phononic crystals. It can consider complex geometry of the structures as well as the inhomogeneity, anisotropy and nonlinearity of the materials. However when the contrast in properties of the component materials is larger, finer mesh is required, which causes large time consumption. And sometimes interesting physical phenomena are shielded if a further analysis of the spectra is not completed by studying the dispersion relation. However the FDTD method cannot give the spectra directly unless inverse Fourier transformation is applied. There are some other methods which are not commonly used, e.g. lumped-mass method (Wang et al. 2004), eigenmode matching theory method (Hou et al. 2004), variational method (Goffaux et al. 2003), finite element method (Zhang et al. 2003), etc. As mentioned above, these methods involve various disadvantages. This makes development of alternative methods of computation desirable.

In recent years, the localization capability and multilevel structure of wavelets have been utilized to develop efficient numerical methods for partial differential equations (PDEs) (Santos et al. 2004; Cohen et al. 2001). The wavelet method, as one of the meshless methods among others (Han and Atluri 2004), has been used in

many boundary-value problems including wave propagation (Mitra and Gopalakrishnan 2006; Zhang 2007; Xiang et al. 2008). Like sine and cosine in Fourier series, wavelets are used as basis functions in representing other functions in series forms. One advantage of wavelets is that they are well localized in both frequency and spatial domains such that they can easily describe the discontinuities. Also, unlike the basis functions in the classical finite element method, wavelets are oscillating functions of the space variables and may be better appropriate to describe spatial oscillations of the wave fields (Checoury and Lourtioz 2006). Moreover, the initial mesh construction is not required and the resulting matrixes are very sparse. In one word, wavelets allow for efficient representations in computation. In other words, wavelets are capable of quickly capturing the essence of a function with only a small set of coefficients.

Checoury and Michel Lourtioz (2006) have recently proposed a wavelet-based method for band structure calculations in 2D photonic crystals by using CDF62 wavelet. Motivated by their research, we try the wavelet-based method for calculating band structures of 2D phononic crystals. A biorthogonal wavelet instead of a CDF62 wavelet, is applied. The main goal of this paper is to extend the work to the phononic structures consisting of general anisotropic materials, mathematically illustrate the advantages of this method in details and list some representative numerical examples for various material combinations (solid-solid, solid-fluid and fluid-fluid) with complex lattice structures (including those with point or line defects) to show the accuracy, fast convergence, wide applicability, etc. The outline of this paper is as follows. In Section 2, we outline the basic theory about multiresolution analyses (MRA), the choice of wavelets, orthogonal wavelets and biorthogonal wavelets. The wavelet algorithm is described in Section 3 and its numerical performance is discussed in Section 4, followed by summary in Section 5.

2 Multiresolution Analysis and Wavelet Bases

We begin with some basic theory and notations to be used throughout this paper. Let Z and R be the set of all integers and real numbers, respectively. Denote $L^2(R) = \{f : \int_R |f(x)|^2 dx < \infty\}$. In Fourier analysis, L^2-functions are represented as linear combinations of trigonometric functions. In the 1980s and 1990s, the wavelet theory was developed on the basis of the Haar's idea (Haar 1910). Wavelet analysis has proved to be an efficient tool in approximation theory since Daubechies (1988), Mallat (1999) and Meyer 1992. It is well known that multiresolution analysis, introduced by Mallat from the signal processing field into mathematics (Mallat 1989), provides a nature framework for the understanding of wavelet bases, and for the construction of wavelets. Therefore, next, we present a brief introduction to the multiresolution analysis to analyze the wavelet bases used in this paper.

2.1 Multiresolution analysis, scaling functions and orthogonal wavelets

A multiresolution analysis of $L^2(R)$ is defined as increasing sequence of closed subspaces $\{V_j\}_{j\in Z} \subset L^2(R)$, that satisfy the following properties

(i) $V_j \subset V_{j+1}, \forall j \in Z, \cap_{j\in Z} V_j = \{0\}, \overline{\cup_{j\in Z} V_j} = L^2(R)$.

(ii) $\forall f \in L^2(R), \forall j \in Z$, we have $f(\cdot) \in V_j \Leftrightarrow f(2^{-j}\cdot) \in V_0$.

(iii) $f \in V_0 \Rightarrow f(\cdot - k) \in V_0, \forall k \in Z$.

(iv) $\exists \phi \in V_0$, such that the sequence $\{\phi(x-k)\}_{k\in Z} = \{\phi_{0,k}(x)\}_{k\in Z}$ is an orthonormal basis (ONB) of the space V_0. The function $\phi(x)$ is called the scaling function of the multiresolution analysis.

Thanks to the conditions (iii) and (iv) it follows that $\phi_{j,k}(x) := 2^{j/2}\phi(2^j x - k), j,k \in Z$ is also an ONB of V_j. If we denote $P_j : L^2(R) \to V_j$, the orthogonal projector operator onto V_j, the condition (i) assures that any $f \in L^2(R)$ can be approximated by its orthogonal projection onto V_j

$$P_j f := \sum_{k\in Z} \langle f, \phi_{j,k} \rangle \phi_{j,k}. \tag{2.1}$$

Then the completeness implies convergence $\lim_{j\to\infty} P_j f = f$.

The main feature of multiresolution analysis is the existence of an orthonormal wavelet basis $\psi_{j,k}(x) \in L^2(R)$, obtained through dilation and translation of the mother wavelet $\psi(x)$, i.e. $\psi_{j,k}(x) := 2^{j/2}\psi(2^j x - k)$ with $j,k \in Z$. In other words, an orthogonal wavelet $\psi(x)$ is simply an L^2-function with some oscillations and a zero average, i.e. $\int_R \psi(x)dx = 0$, such that wavelets have rapid decay or compact supports, and hence have good localization capability, whereas the sine and cosine used in Fourier analysis are harmonic waves spreading over the whole real line and lack the aforementioned capability.

By applying projecting theorem on Hilbert space, we obtain the following equality

$$V_{j+1} = V_j \oplus W_j. \tag{2.2}$$

Where the wavelet space W_j is the orthogonal complement of V_j in the space V_{j+1}, such that by fixing $j \in Z$, $\{\psi_{j,k}(x)\}_{k\in Z}$ is an orthonormal basis of W_j.

Similarly, let $Q_j : L^2(R) \to W_j$ be the orthogonal projection defined by

$$Q_j f := \sum_{k\in Z} \langle f, \psi_{j,k} \rangle \psi_{j,k}. \tag{2.3}$$

Then considering Eq.(2.2) , we find a link between the approximation function on V_j, and the approximation function on V_{j+1}

$$P_{j+1}f = P_j f + Q_j f. \tag{2.4}$$

Obviously, $P_{j+1}f$ approximates f at a finer scale than $P_j f$ does. In other words, $P_{j+1}f$ reveals more details, which are represented by the wavelet terms in $Q_j f$.

Since $\phi, \psi \in V_0 \subset V_1$ and $\{\phi_{1,k} | k \in Z\}$ is an ONB of V_1, we have a pair of filter $h = \langle h_n \rangle_{n\in Z}$, $g = \langle g_n \rangle_{n\in Z}$, such that

$$\phi = \sum_{n\in Z} h_n \phi_{1,n}, \quad \psi = \sum_{n\in Z} g_n \phi_{1,n}, \quad g_n = (-1)^n h_{1-n} \tag{2.5}$$

From Eq. (2.5), we have

$$\begin{aligned}
\phi_{j,k}(x) &= 2^{j/2}\phi(2^j x - k) = 2^{j/2} \sum_{n\in Z} h_n \phi_{1,n}(2^j x - k) \\
&= \sum_n h_n 2^{(j+1)/2} \phi(2^{j+1}x - (2k+n)) \\
\psi_{j,k}(x) &= 2^{j/2}\psi(2^j x - k) = 2^{j/2} \sum_{n\in Z} g_n \phi_{1,n}(2^j x - k) \\
&= \sum_n g_n 2^{(j+1)/2} \phi(2^{j+1}x - (2k+n))
\end{aligned}$$

Let $m = 2k+n$, then we get

$$\phi_{j,k}(x) = \sum_m h_{m-2k} \phi_{j+1,m}(x), \quad \psi_{j,k}(x) = \sum_m g_{m-2k} \phi_{j+1,m}(x) \tag{2.6}$$

Set $a_{j,k} = \langle f, \phi_{j,k} \rangle = \int_{-\infty}^{+\infty} f(x)\overline{\phi_{j,k}(x)}dx$ and $b_{j,k} = \langle f, \psi_{j,k} \rangle = \int_{-\infty}^{+\infty} f(x)\overline{\psi_{j,k}(x)}dx$, then Eq. (2.6) leads to the following decomposition algorithm connecting coefficients of successive approximations:

$$a_{j,k} = \sum_m h_{m-2k} \alpha_{j+1,k}, b_{j,k} = \sum_m g_{m-2k} \alpha_{j+1,k}. \tag{2.7}$$

Moreover, from Eq. (2.6), the orthogonality implies that $\langle \phi_{j,m}, \phi_{j+1,k} \rangle = h_{k-2m}$ and $\langle \psi_{j,m}, \phi_{j+1,k} \rangle = g_{k-2m}$. Then considering the definition of orthogonal projection and Eq. (2.4), we get the reconstruction algorithm

$$\begin{aligned}
a_{j+1,k} &= \langle f, \phi_{j+1,k} \rangle = \langle P_{j+1}f, \phi_{j+1,k} \rangle = \langle P_j f, \phi_{j+1,k} \rangle + \langle Q_j f, \phi_{j+1,k} \rangle \\
&= \sum_m a_{j,m} \langle \phi_{j,m}, \phi_{j+1,k} \rangle + \sum_m b_{j,m} \langle \psi_{j,m}, \phi_{j+1,k} \rangle \\
&= \sum_m h_{k-2m} a_{j,m} + \sum_m g_{k-2m} b_{j,m}
\end{aligned} \tag{2.8}$$

Let $j_0 < J$ be the selected coarsest and finest resolution levels, then applying Eqs. (2.2) and (2.4) recursively yields

$$V_J = V_{j_0} \oplus W_{j_0} \oplus \cdots \oplus W_{J-1} \tag{2.9}$$

and

$$f \approx \sum_k \langle f, \phi_{J,k} \rangle \phi_{J,k} = \sum_k \langle f, \phi_{j_0,k} \rangle \phi_{j_0,k} + \sum_{j=j_0}^{J-1} \sum_k \langle f, \psi_{j,k} \rangle \psi_{j,k}. \tag{2.10}$$

This motivates us to carry out a progressive multilevel approximation. We first approximate the function from a coarse level, and then add in more details level by level through wavelet terms if necessary. In addition, wavelet coefficients in the smooth regions of a function will be small and thus can be neglected to save computations and storage. In other words, compression in the wavelet decomposition can be performed to improve the efficiency of approximation.

The periodic wavelet can be derived from the MRA in the real line mentioned above. Suppose $j \in Z_+, k = 0, ..., 2^j - 1$, we define

$$\phi_{j,k}^{(period)}(x) := \sum_{p \in Z} \phi_{j,k}(x-p),$$

$$V_j^{(period)} := span\{ \phi_{j,k}^{(period)}(x) \Big| k = 0, ..., 2^j - 1\}$$

$$\psi_{j,k}^{(period)}(x) := \sum_{p \in Z} \psi_{j,k}(x-p),$$

$$W_j^{(period)} := span\{ \psi_{j,k}^{(period)}(x) \Big| k = 0, ..., 2^j - 1\}.$$

Then $\{V_j^{(period)}\}_{j \in Z_+}$ forms a periodic multiresolution analysis (PMRA) in $L^2([0,\ 1])$, and $\{ \phi_{j,k}^{(period)}(x) \Big| k = 0, ..., 2^j - 1\}$ and $\{ \psi_{j,k}^{(period)}(x) \Big| k = 0, ..., 2^j - 1\}$ are respectively an ONB of $V_j^{(period)}$ and $W_j^{(period)}$ with $V_j^{(period)} \oplus W_j^{(period)} = V_{j+1}^{(period)}$.

The properties of the scaling function and wavelet affect the performance of approximation in various aspects. The lengths of their supports determine computation cost. The number of vanishing moments of the wavelet implies compression potential. Given the number of vanishing moments, Daubechies wavelets have the minimal support length. In this aspect, they are optimal and hence popular in applications. As we know, in Fourier analysis, L^2-functions are represented as linear combinations of sines and cosines. However, unlike the Fourier analysis where only trigonometric function bases are adopted, the wavelet analysis has

many different function families to choose, and in the same wavelet function family there exist different order wavelet functions. On one hand, this enhances the ability of solving different problems; on the other hand, the appropriate choice of the best wavelet basis must be considered for different problems. In general, four different wavelet families such as Daubechies wavelets, Coiflets wavelets, Symlets wavelets and biorthogonal wavelets are usually used in different fields. Here, we considered the most representative Daubechies wavelets families and biorthogonal wavelet families from the approximation-oriented points of view. Mathematically, the essence of compression is to use the least wavelet series terms to approximate the original function. Generally the basis functions are more similar to the original function, the less wavelet series terms are necessary to approximate the original function. Usually, the Daubechies wavelets which are often employed in some literatures do not hold the best compressibility, but biorthogonal wavelets do. Therefore in this paper, considering the definite calculation of the phononic crystals, we adopt the biorthogonal wavelet. User et al. (1996, 1998) compared the approximation ability of the biorthogonal wavelet families and Daubechies wavelet functions families and showed mathematically that the biorthogonal functions have the better approximation ability than that of the Daubechies wavelet for the smooth functions. Moreover, Daubechies wavelet functions are not symmetric. In contrast, the biorthogonal wavelet families have the strict symmetry. Thus for the periodic structures, we prefer to choose the wavelet with symmetry and antisymmetry properties because the edge disposal is very convenient and the function distortion is the least in the reconstruction. And, the advantages of biorthogonal wavelets are also discussed in Ewing et al. 2004. In addition, we remind that the periodic wavelet bases are used in our periodic problems. The periodized wavelets and their scaling functions possess the similar properties of their non-periodic counterparts, e.g. orthonormality and biorthogonality as discussed in this paper.

2.2 Biorthogonal wavelets

As discussed above, biorthogonal wavelets were motivated by concerns about exact reconstruction and symmetry in signal processing and developed to improve the shortcomings of orthogonal wavelets while maintaining their advantages. For ease of exposure, we begin with the one-dimensional (1D) case. The analysis process may be directly extended to the two-dimensional (2D) or higher-dimensional case in a straightforward manner.

Usually, biorthogonal wavelets are connected with biorthogonal MRA. A biorthogonal MRA is the sequence of closed subspaces in $L^2(R)$, i.e.

$$V_j \subset V_{j+1}, \quad \tilde{V}_j \subset \tilde{V}_{j+1}, \quad W_j \subset W_{j+1}, \quad \tilde{W}_j \subset \tilde{W}_{j+1} \tag{2.11}$$

Set

$$\begin{aligned} V_j &= span\{\phi_{j,k} \big| k \in Z\}, \quad W_j = span\{\psi_{j,k} \big| k \in Z\} \\ \tilde{V}_j &= span\{\tilde{\phi}_{j,k} \big| k \in Z\}, \quad \tilde{W}_j = span\{\tilde{\psi}_{j,k} \big| k \in Z\} \end{aligned} \tag{2.12}$$

Considering Eq. (2.11), it is apparent that the following relations hold

$$V_{j+1} = V_j + W_j, \tilde{V}_{j+1} = \tilde{V}_j + \tilde{W}_j. \tag{2.13}$$

$$V_j \perp \tilde{W}_{j'}, \quad \tilde{V}_j \perp W_{j'}, \quad \text{for } j \leq j' \tag{2.14}$$

Now we construct biorthogonal wavelets and scaling functions from two pairs of filters (h_n, g_n) and $\left(\tilde{h}_n, \tilde{g}_n\right)$ through two-scale equations

$$\phi = \sum_{n \in Z} h_n \phi_{1,n}, \psi = \sum_{n \in Z} g_n \phi_{1,n}, \quad \tilde{\phi} = \sum_{n \in Z} \tilde{h}_n \tilde{\phi}_{1,n}, \quad \tilde{\psi} = \sum_{n \in Z} \tilde{g}_n \tilde{\phi}_{1,n}$$

where ϕ and $\tilde{\phi}$ are called the primal scaling function and dual scaling function, respectively; and ψ and $\tilde{\psi}$ are called the primal wavelet and dual wavelet, respectively. It is noted that the roles of these two pairs of filters are symmetric and can be switched. The same is true for the primals and duals.

From Eq. (2.5), again, we have the choices for g_n and $\tilde{g}_n$

$$g_n = (-1)^n \tilde{h}_{1-n}, \tilde{g}_n = (-1)^n h_{1-n} \tag{2.15}$$

An important property of the biorthogonal wavelet is the following biorthogonal relations:

$$\left\langle \phi_{0,k}, \tilde{\phi}_{0,k'} \right\rangle = \delta_{k,k'} \tag{2.16}$$

$$\left\langle \psi_{j,k}, \tilde{\psi}_{j',k'} \right\rangle = \delta_{j,j'} \delta_{k,k'} \tag{2.17}$$

For any $f \in L^2(R)$, we may choose a coarse resolution level j_0 and a fine level $J(>j_0)$ to carry out one-level or multilevel approximations similar to the orthogonal case

$$f = \sum_k \left\langle f, \tilde{\phi}_{J,k} \right\rangle \phi_{J,k} = \sum_k \left\langle f, \tilde{\phi}_{j_0,k} \right\rangle \phi_{j_0,k} + \sum_{j=j_0}^{J-1} \sum_k \left\langle f, \tilde{\psi}_{j,k} \right\rangle \psi_{j,k}. \tag{2.18}$$

Eq. (2.18) indicates that the function may be decomposed by the primal functions and reconstructed by the dual functions. One may also use the dual functions for decomposition and the primal functions for reconstruction.

Most orthogonal scaling functions and wavelets do not have explicit expressions, which is an obvious shortcoming for their applications in some situations. In this

sense, biorthogonal spline wavelets are appealing since the primal scaling function and wavelet are splines, and hence have explicit expressions and known regularities. Therefore, numerical methods built upon biorthogonal spline wavelets possess some known regularities, and thus possess some features of the traditional finite element methods besides the advantage of the multilevel structure.

Here, the Haar wavelet (i.e. Bior(1,1)), Bior(2,8) and Bior(3,9) are plotted in Fig.1 and will be used in our numerical experiments. The detailed definition and properties of biorthogonal wavelet are referred to Cohen et al. 1992.

3 Description of the Algorithm

The algorithm is developed within the variational principle framework. The theory and practice of such methods for elliptic problems are rather well understood. For details, we refer to the corresponding literatures (Ciarlet 1978). We will only describe here the 2D case. The 3D case is handled similarly.

3.1 Problem formulation

Consider Eq. (1.1), $\rho(\mathbf{r})$ and $\mathbb{C}(\mathbf{x})$ are the space-dependent periodic functions. The algorithm handles arbitrary lattices of periods. Treatment of periodic problems requires utilization of the so-called Floquet-Bloch theory (Eastham 1973 for its description in the case of partial differential equations and Ashcroft and Mermin 1976 for its applications in solid state physics). Based on the Bloch theorem, the elastic displacements can be written in the following form

$$\mathbf{u}(\mathbf{r}) = e^{i(\mathbf{k}\cdot\mathbf{r})}\mathbf{u}_{\mathbf{k}}(\mathbf{r}) \tag{3.1}$$

where $\mathbf{u}_{\mathbf{k}}(\mathbf{r})$ are two-dimensional and periodic; $i=\sqrt{-1}$; and $\mathbf{k}=(k_x,k_y)$ is a 2D wave vector contained in the first Brillouin Zone (BZ) of the reciprocal lattice. Substituting (3.1) into (1.1), we obtain

$$(\nabla + i\mathbf{k})\cdot[\mathbb{C}:(\nabla + i\mathbf{k})\otimes\mathbf{u}_{\mathbf{k}}(\mathbf{r})] = -\rho(\mathbf{r})\omega^2\mathbf{u}_{\mathbf{k}}(\mathbf{r}). \tag{3.2}$$

Eq. (3.2) can be rewritten in a variational form as

$$\langle v,\ (\nabla + i\mathbf{k})\cdot[\mathbb{C}:(\nabla + i\mathbf{k})\otimes\mathbf{u}_{\mathbf{k}}(\mathbf{r})]\rangle = -\omega^2\langle v,\ \rho(\mathbf{r})\mathbf{u}_{\mathbf{k}}(\mathbf{r})\rangle, \quad \forall v\in L^2(\Omega) \tag{3.3}$$

where v is an arbitrary square integrable function. Equivalently, (3.3) may be written in the integral form

$$\int_{\Omega}\mathbb{C}:(\nabla + i\mathbf{k})\otimes\mathbf{u}_{\mathbf{k}}(\mathbf{r})\cdot\overline{(\nabla + i\mathbf{k})v}d\mathbf{r} = \omega^2\int_{\Omega}\rho(\mathbf{r})\mathbf{u}_{\mathbf{k}}(\mathbf{r})\bar{v}d\mathbf{r}. \tag{3.4}$$

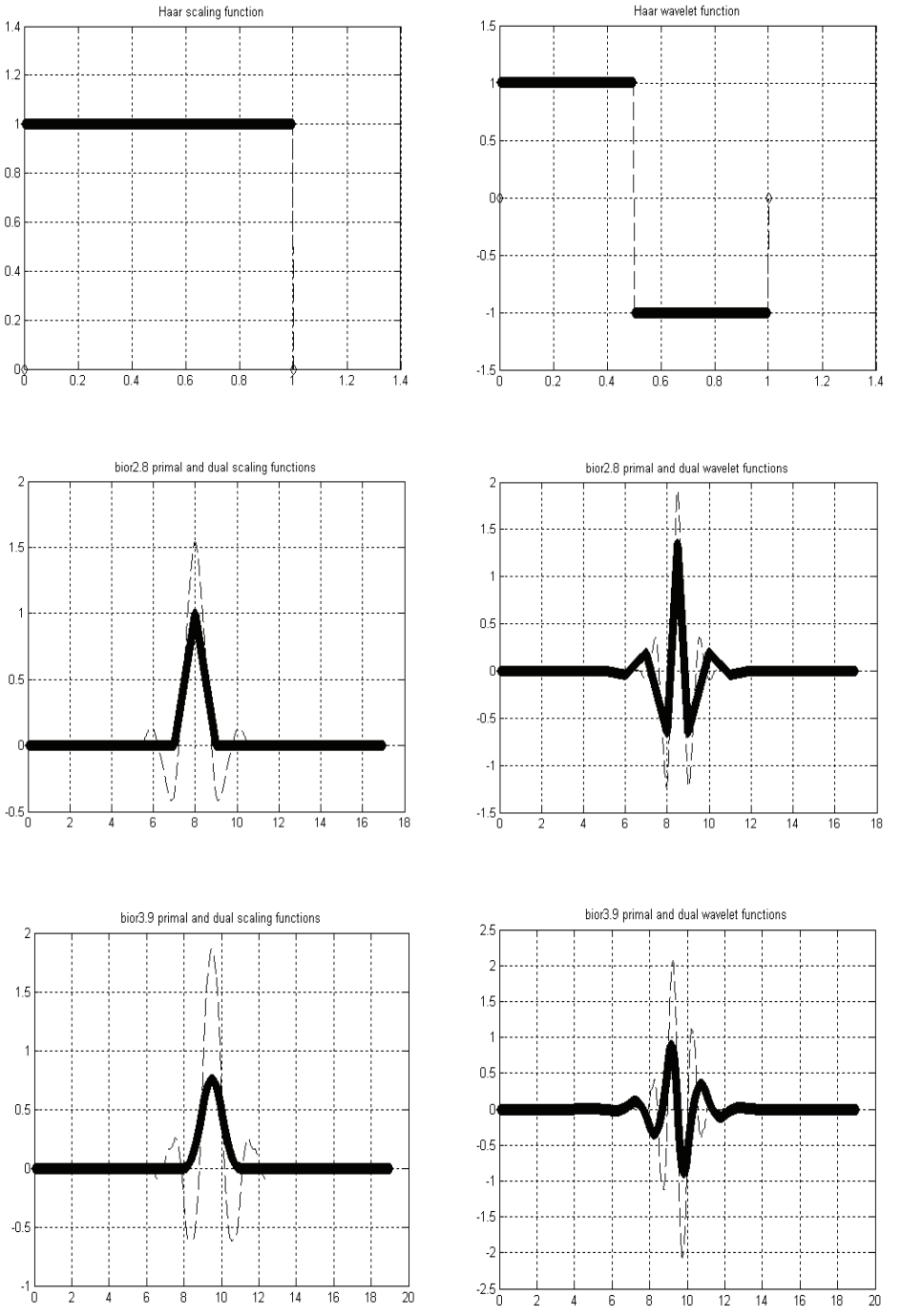

Figure 1: Haar and Biorthogonal scaling functions and wavelets, Bior(2,8) and Bior(3,9)

Due to the spatial periodicity, $\mathbf{u_k}(\mathbf{r})$ and the material constants, $\rho(\mathbf{r})$ and $\mathbb{C}(\mathbf{x})$, can be expanded in biorthogonal wavelet basis and Haar wavelet basis, respectively (see Section 2)

$$\mathbf{u_k}(\mathbf{r}) = \sum_{b_m \in \Psi_{j_0,J}} \hat{\mathbf{u}}_{\mathbf{k},m} b_m \tag{3.5}$$

$$\alpha(\mathbf{r}) = \sum_{d_m \in \Psi_{j_0,J}} \hat{\alpha}_{\mathbf{k},m} d_m \tag{3.6}$$

where $\alpha(\mathbf{r}) = (\rho(\mathbf{r}), \mathbb{C}(\mathbf{r}))$; $\hat{\alpha}_{\mathbf{k},m}$ and $\hat{\mathbf{u}}_{\mathbf{k},m}$ are the corresponding wavelet coefficients; and the localized basis set is

$$\begin{aligned}&\Big\{\varphi^{period}_{j_0,k1,k2} :\ k1 = 0,...,2^{j_0}-1;\ k2 = 0,...,2^{j_0}-1\Big\}\\ &\cup\Big\{\psi^{(\lambda),period}_{j,k1,k2} :\ \lambda = 1,2,3;\ k1 = 0,...,2^{j}-1;\ k2 = 0,...,2^{j}-1;\ j = j_0,...,J-1\Big\}.\end{aligned} \tag{3.7}$$

Each function in this set is the 2D periodic wavelets and scaling functions consisting of a product of two 1D periodic wavelets and scaling functions (see figure 1). It is understood that different wavelet basis may be selected for $\rho(\mathbf{r})$, $\mathbb{C}(\mathbf{x})$ and $\mathbf{u_k}(\mathbf{r})$. The integer J fixes the approximation degree and the maximum number 2^{2J} of the wavelets and scaling basis functions used in the expansion. An adaptive algorithm would add or remove wavelets during calculations without restriction on the integer J and would stop when a desired accuracy is obtained.

Substituting Eq (3.5) into Eq. (3.4), and then choosing the square integrable function $v = b_q$, we obtain

$$\int_\Omega \mathbb{C} : [(\nabla + i\mathbf{k}) \otimes \hat{\mathbf{u}}_{\mathbf{k},p} b_p] \cdot \overline{(\nabla + i\mathbf{k})} \tilde{b}_q d\mathbf{r} = \omega^2 \int_\Omega \rho(\mathbf{x}) \hat{\mathbf{u}}_{\mathbf{k},p} b_p \tilde{b}_q d\mathbf{r} \tag{3.8}$$

As stated in Section 2, an arbitrary function $f \in L^2[0,1]$ may be approximated by the wavelet series at a given j_0 scale and a complementary part at a finer scale [see Eq. (2.10)],

$$f(x) = \sum_{k=0}^{2^{j_0}-1} s_k \varphi^{period}_{j_0,k}(x) + \sum_{\substack{j \in Z \\ j \geq j_0}} \sum_{k=0}^{2^j-1} d_{j,k} \psi^{period}_{j,k}(x), \quad x \in [0,\ 1], \tag{3.9}$$

where $\mathbf{k}$ is the location in space. One can change the scale of the function by changing the truncation of the series in j to improve the accuracy of the approximation.

Considering the fact that $\rho(\mathbf{r})$ and $\mathbb{C}(\mathbf{r})$ are all piecewise constant functions, we will use the periodic Haar wavelets to represent them. As for the displacement fields we will try the periodic Bior3.9 wavelets which involve more vanishing moments than Bior2.8 wavelets. The advantages of using these wavelets have been demonstrated in Section 2.

Haar wavelet is a step function. It is the only one compactly supported, orthogonal and symmetric wavelet and is well adapted to the piecewise constant functions. Eq. (3.9), which is now supposed to represent $\rho(\mathbf{r})$ and $\mathbb{C}(\mathbf{r})$, may be expanded in the form of the periodic Haar wavelets and scaling functions,

$$f^{Haar}(x) = \sum_{k=0}^{2^{j_0}-1} s_k \varphi_{j_0,k}^{period,Haar}(x) + \sum_{\substack{j\in Z \\ j\geq j_0}} \sum_{k=0}^{2^j-1} d_{j,k} \psi_{j,k}^{period,Haar}(x), \tag{3.10}$$

where the wavelet coefficients

$$s_k = \left\langle \varphi_{j_0,k}^{period,Haar}, f^{Haar} \right\rangle \text{ and } d_{j,k} = \left\langle \psi_{j,k}^{period,Haar}, f^{Haar} \right\rangle.$$

When expanding the phononic crystal displacements in the wavelets, we expect that they can be represented accurately with as few coefficients as possible. Here, we will use the periodic Bior3.9 wavelets. Similarly Eq. (3.9), which is now supposed to represent displacements, may be expanded in the following form

$$f^{bior3.9}(x) = \sum_{k=0}^{2^{j_0}-1} s_k \tilde{\varphi}_{j_0,k}^{period,bior3.9}(x) + \sum_{\substack{j\in Z \\ j\geq j_0}} \sum_{k=0}^{2^j-1} d_{j,k} \tilde{\psi}_{j,k}^{period,bior3.9}(x), \tag{3.11}$$

where the wavelet coefficients

$$s_k = \left\langle \varphi_{j_0,k}^{period,bior3.9}, f^{bior3.9} \right\rangle \text{ and } d_{j,k} = \left\langle \psi_{j,k}^{period,bior3.9}, f^{bior3.9} \right\rangle.$$

The above equation indicates that the function $f^{bior3.9}(x)$ may be decomposed by the primal functions and reconstructed by the dual functions.

The above formulation, Eqs. (3.9)-(3.11), is for 1D periodic systems. To calculate the elastic band structures of 2D phononic crystals, we must use 2D wavelets defined on $[0,1]\otimes[0,1]$. (Bi)orthogonal wavelets on $[0,1]\otimes[0,1]$ are generated by periodizing compactly supported wavelets on $R\otimes R$ via tensor products. For example, Figure 2 shows the 2D Haar scaling function, $\varphi(x,y)=\varphi(x)\varphi(y)$, and the three wavelet functions, $\psi^{(1)}(x,y)=\varphi(x)\psi(y)$, $\psi^{(2)}(x,y)=\psi(x)\varphi(y)$ and $\psi^{(3)}(x,y)=\psi(x)\psi(y)$, resulting from the tensor products of the 1D Haar scaling and wavelet

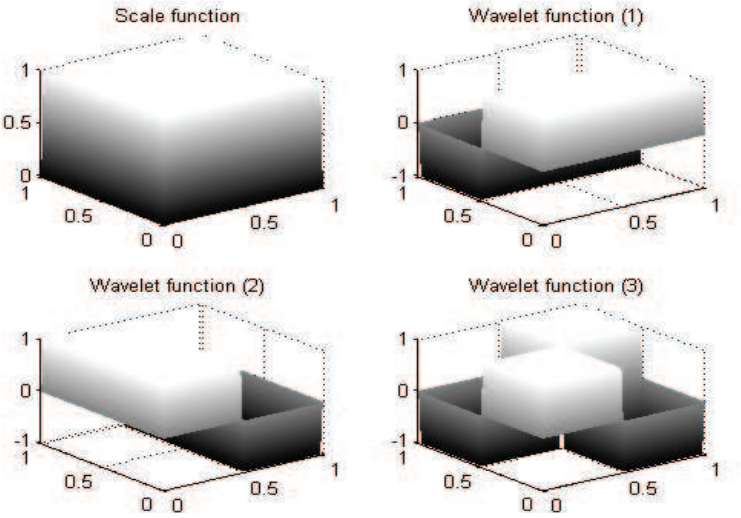

Figure 2: A 2D Haar scaling function and three wavelet functions

functions. An arbitrary 2D periodic function $f(x,y)$ can be expanded in the 2D periodic wavelets, e.g.,

$$f(x,y) = \sum_{k1=0}^{2^{j_0}-1} \sum_{k2=0}^{2^{j_0}-1} \chi_{k1,k2} \varphi_{j_0,k1,k2}^{period}(x,y) + \sum_{\substack{j\in Z \\ j\geq j_0}} \sum_{k1=0}^{2^j-1} \sum_{k2=0}^{2^j-1} \gamma_{j,k1,k2} \psi_{j,k1,k2}^{(\lambda)period}(x,y),$$

$$\lambda = 1,2,3,\ x,y \in [0,1] \quad (3.12)$$

where the coefficients $\chi_{k1,k2}$ and $\gamma_{j,k1,k2}$ are defined in similar way to those in Eqs. (3.10) and (3.11).

Eq. (3.8) may be rewritten in a compact form

$$\mathbf{M} \cdot \hat{\mathbf{u}}_{\mathbf{k}} = \omega^2 B \cdot \hat{\mathbf{u}}_{\mathbf{k}} \quad (3.13)$$

where $\mathbf{M}$ and $\mathbf{B}$ are sparse matrices and $\hat{\mathbf{u}}_{\mathbf{k}}$ the column vector containing $\hat{\mathbf{u}}_{x\mathbf{k}}$, $\hat{\mathbf{u}}_{y\mathbf{k}}$ and $\hat{u}_{z\mathbf{k}}$. The elements of these matrices are

$$(\mathbf{M})_{p,q} = \int_{\Omega} \mathbb{C} : [(\nabla + i\mathbf{k})b_p] \cdot \overline{(\nabla + i\mathbf{k})\tilde{b}_q} d\mathbf{r} \quad (3.14)$$

$$(\mathbf{B})_{p,q} = \int_{\Omega} \rho(\mathbf{r}) b_p \tilde{b}_q d\mathbf{r} \quad (3.15)$$

Eq. (3.13) leads to the eigenvalue problem. Numerical solution to this problem can be conducted by truncating the series in j to J-th terms, i.e. $j = j_0, ..., J-1$. The eigenvalues of (3.13) considered as functions of $\mathbf{k}$ are called band functions or dispersion relations. The union of ranges of all band functions forms the spectrum of the original problem.

If the plane (x, y) is a symmetric plane of the anisotropic system, the in-plane and out-of-plane wave modes are uncoupled and can be solved separately from the eigenvalue equation (3.13).

3.2 Assembling and storage of the matrices

Computation of matrices $\mathbf{M}$ and $\mathbf{B}$ is straightforward according to the formulas introduced above. This involves the computation of the wavelet integrals. For example, on substitution of the periodic Haar wavelet expansions of the functions $\rho(\mathbf{r})$ and $\mathbb{C}(\mathbf{r})$ into Eqs. (3.14) and (3.15), $(\mathbf{M})_{p,q}$ can be expressed as a linear combination of the wavelet integrals with the form

$$\int_{\Omega} \psi^{period,Haar}(\mathbf{r})(\nabla + i\mathbf{k})b_p \cdot \overline{(\nabla + i\mathbf{k})}\widetilde{b}_q d\mathbf{r}, \tag{3.16}$$

which are independent of the particular forms of $\rho(\mathbf{r})$ and $\mathbb{C}(\mathbf{r})$ and therefore can be computed with high accuracy once for all. The basic idea is that the computation of the wavelet integrals on general decomposable domains can be reduced to the computation of the similar integrals on the unit interval (i.e. [0, 1]). In this reduction process, suitable approximations are introduced to make the computation efficient. The construction on a fairly general domain Ω is achieved by the following steps

$$R \to [0,1] \to [0,1]^2 \to \Omega = \bigcup \Omega_i, \quad \Omega_i \sim [0,\ 1]^2, \tag{3.17}$$

where the first step is completed by restriction and adaptations at the edges, the second step by tensor product, and the third step by domain decomposition techniques.

The key point for the wavelet integral in Eq. (3. 16) mainly relies on the two-scale relation for the wavelets and scaling functions (see Niklasson et al. 2002 and Bertoluzza 2000 and references therein).

3.3 Solution of the generalized eigenvalue problem

The choice of a proper method for solving the generalized eigenvalue problem (3.13) is also very important. In computing band structures of phononic crystals, one is usually interested only in a small number (up to 10) of the lowest eigenvalues. Thus we expect a method that provides calculation of only such eigenvalues rather

than attempting to compute all of them, and that efficiently utilizes sparseness of matrices involved. The classical iterative method is known to have these properties and can solve the eigenproblems faster than a direct solution. They usually need a good starting point for iteration as well as the knowledge of a good preconditioner (i.e. an approximate inverse of the matrix $\mathbf{M}$). Here we will now briefly describe the algortithm (for details we refer to David 2002). For a given scale J, the eigenvectors of the sub-matrix M_k^{J-1} can be used as the initial value to calculate the eigenvalue problem of the matrix M_k^J because M_k^{J-1} may be regarded as a first order approximation of M_k^J. The detailed preconditioning and adaptability of the matrix M_k^J can be referred to Cohen and Masson 1999. In this paper, we choose the preconditioning of the matrix M_k^J as $\begin{pmatrix} (M_k^{j_0}) & 0 \\ 0 & \mathrm{dia}D_{k,J} \end{pmatrix}^{-1}$ (see Cohen and Masson 1999). Obviously, the dimension of the diagonal matrix $\mathrm{dia}D_{k,J} = (m_{d,d})$ is $(2^{2J} - 2^{2j_0}) \times (2^{2J} - 2^{2j_0})$ where $m_{d,d}$ are the diagonal elements of matrix M_k^J with $2^{2j_0} < d \leq 2^{2J}$. So, we may easily compute the preconditioner since the inverse of the matrix $M_k^{j_0}$ is relatively smaller than M_k^J.

4 Performance of the Algorithm

In this section, we will illustrate the performance of the developed method for several typical 2D phononic crystals with or without defects. The calculations were implemented on a personal computer with a Pentium4, 2.5GHz CPU and 256MB memory. In order to check whether the algorithm works correctly and efficiently, we have tested it against several typical cases with different lattice structures, scatterer shapes and material combinations.

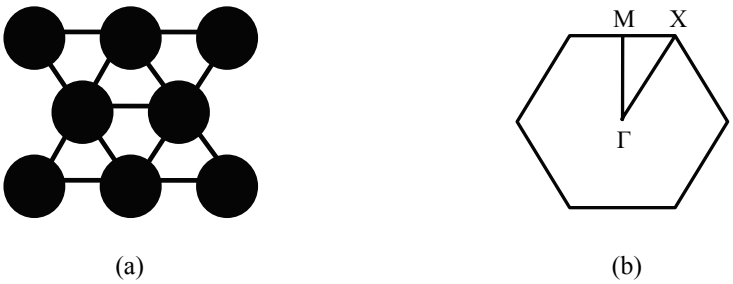

(a) (b)

Figure 3: The transverse cross-section (a) and the first Brillouin zone (b) of the 2D triangular lattice

Two typical lattice structures—triangular and square, and two kinds of scatterer cross-sections —circular and square are calculated. Figs. 3 and 4 show, respec-

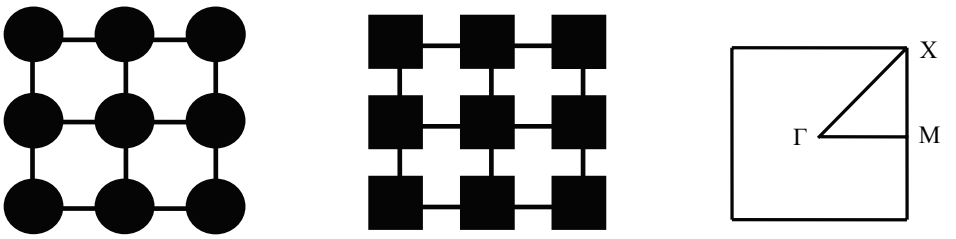

(a) (b) (c)

Figure 4: The transverse cross-sections (a,b) and the first Brillouin zone (c) of the 2D square lattice

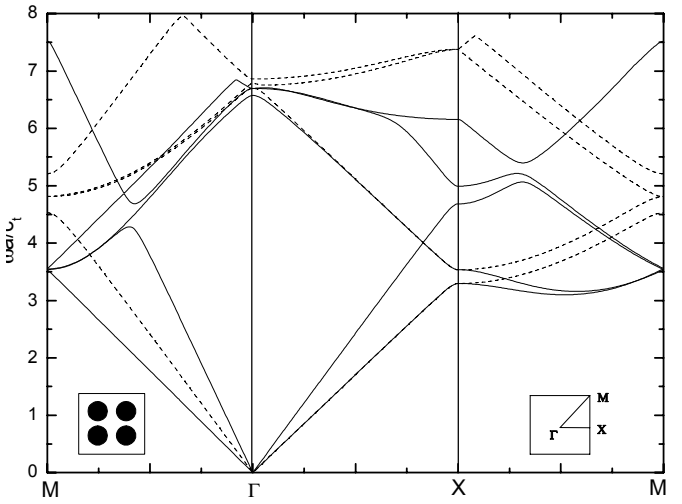

Figure 5: Band structures for a square lattice of AlAs circular columns embedded in GaAs with general anisotropy. The solid curves are for the in-plane modes and the dashed curves for the out-of-plane modes

tively, the transverse cross-sections and the first Brillouin zones of the triangular and square lattices.

4.1 Solid-solid systems

We first check the validity of the present method for anisotropic material combinations by considering a square lattice of AlAs circular columns embedded in GaAs which was studied in Tanaka and Tamura (1998) with the PWE method. The mate-

rial constants may be found in the reference. In calculation, we take 4096 wavelet basis functions. The results of the first few band structures are shown in Fig. 5. These results agree well with those obtained by the PWE method (see Fig.1 in Tanaka and Tamura 1998). That is to say, the wavelet method can yield the same results as the PWE method.

To check the accuracy and convergence of the present method, we perform the detailed computation for a system with large acoustic mismatch. Here we take the isotropic material combinations of Au/Epoxy with different lattice structures and scatterer shapes. The material parameters are $\rho_{gold} = 19500\text{kg/m}^3$, $\rho_{epo} = 1180\text{kg/m}^3$, $c_{l,gold} = 3360\text{m/s}$, $c_{l,epo} = 2535\text{m/s}$, $c_{t,gold} = 1239\text{m/s}$, $c_{t,epo} = 1157\text{m/s}$. The filling fraction is $f = 0.4$. Fig. 6 illustrates the band structures in the first Brillouin zone for the triangle lattice with the circular scatterers (Fig. 6a), the square lattice with the circular scatterers (Fig. 6b) and the square lattice with the square scatterers (Fig. 6c). The frequencies are measured in the dimensionless unit $\omega a/2\pi c_{t,epo}$. The solid lines represent the in-plane modes and the dashed lines show the out-of-plane modes. For comparison, the results obtained with the PWE method (see Kushawaha 1999) are represented by the scattered solid circles for the in-plane modes and by the scattered hollow circles for the out-of-plane modes. The results by these two methods are identical. In calculation, we take 1024 wavelet basis functions and 1089 plane waves. Table 1 lists the frequency regions of the first three spectral bands for the last case (the square lattice with the square scatterers), which numerically shows the satisfied agreement between the two methods.

Table 1: Frequency regions of the first three spectral bands for the square lattice with the square scatterers

Band No.	In-plane modes	
	PWE method	Wavelet method
1	[0, 0.34476]	[0, 0.33348]
2	[0, 0.37091]	[0, 0.3541]
3	[0.34615, 0.40714]	[0.33587, 0.39699]
Band No.	Out-of-plane modes	
	PWE method	Wavelet method
1	[0, 0.25]	[0, 0.2356]
2	[0.7806, 0.87364]	[0.77101, 0.86334]
3	[0.8381, 0.89029]	[0.8277, 0.8801]

To verify the convergence of the developed method, we define a relative error of the eigenfrequency as $\delta_{k,n} = \left|\omega_{k,n} - \omega_{k,n,ref}\right| / \omega_{k,n,ref}$, where the referenced value $\omega_{k,n,ref}$ is the eigenfrequency with 4096 wavelet basis functions. The relative errors

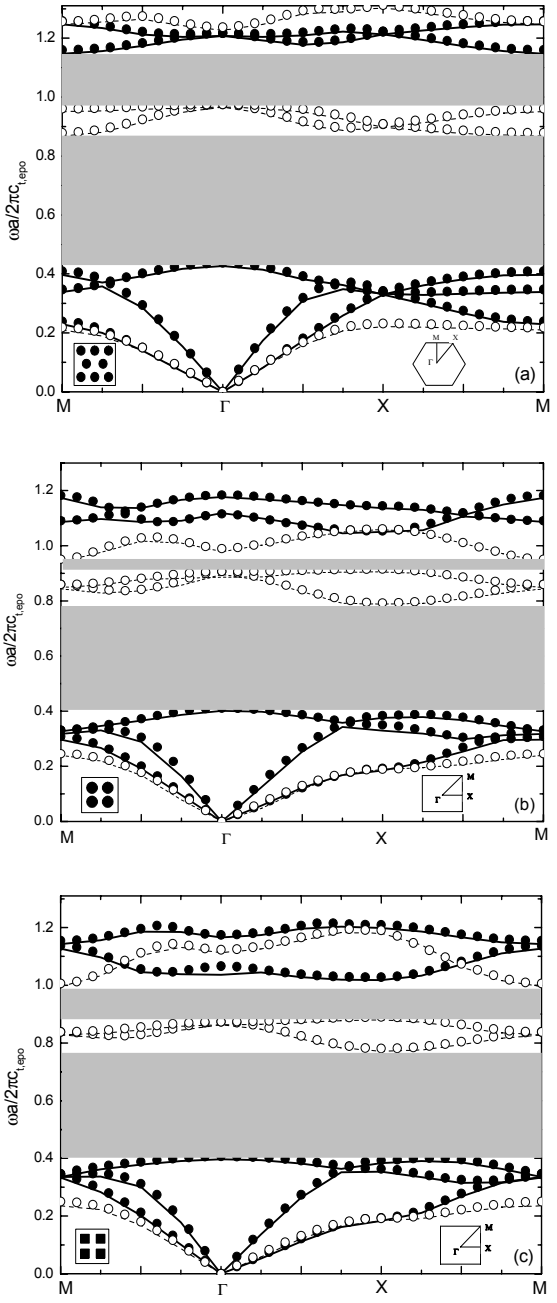

Figure 6: Band structures for Au/Epoxy systems: (a) triangular lattice of circular scatterers; (b) square lattice of circular scatterers; and (c) square lattice of square scatterers. The lines are from the wavelet method, and the scattered symbols from the PWE method

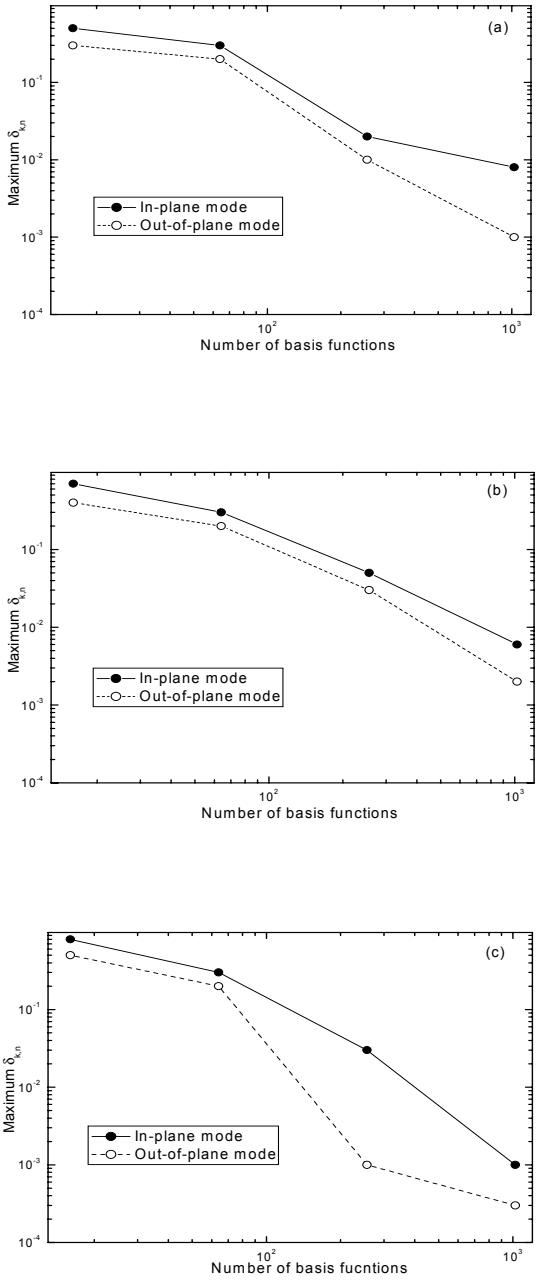

Figure 7: Convergence of the wavelet method, maximum relative error versus the number of wavelet basis functions: (a) triangular lattice of circular scatterers; (b) square lattice of circular scatterers; (c) square lattice of square scatterers

were calculated for the first 8 eigenmodes ($1 \leq n \leq 8$) with arbitrary k by selecting various numbers (smaller than 4096) of the basis functions. Then we choose the maximum values (i.e. $\max_{1\leq n\leq 8,\forall \mathbf{k}} \{\delta_{k,n}\}$) and plot them versus the number of basis functions in Fig. 7 which is corresponding to the band structures in Fig. 6 for the three systems. It is seen that the algorithm converges faster for the out-of-plane modes than for the in-plane modes. This is due to the fact that the in-plane motion involves a higher order system of the eigenvalue problem. The algorithm exhibits the similar convergence for both triangular and square lattices with circular scatterers (see Figs. 7a and 7b). However, one may find that the convergence for the square lattice with square scatterers (Fig. 7c) is faster than that for the other two cases (Figs. 7a and 7b). The reason is related to the choice of the basis functions which are actually the products of two Bior3.9 functions, one depending only on x and the other on y (see section 3). A smaller number of wavelets is then needed to describe the wave fields in the square (x,y) geometry than in the circular one.

4.2 Mixed solid-fliud systems

The PWE method works poorly for mixed solid-fluid systems because of the complex wave modes ranging from the longitudinal modes in the fluid to the mixed longitudinal and transverse modes in the solid (Li et al. 2003). For the system with the solid scatterers in the fluid matrix, the PWE method may yield the results well approximately by imposing the rigid condition to the scatterers. However, for the system of the solid host with holes filled with the fluid, an artificial transverse speed must be assumed in the fluid when the PWE method is used, otherwise it fails to give correct results (Goffaux and Vigneron 2001). Even though, the computed results are very much sensitive to the choice of the artificial transverse speed which is not a trivial task. In addition, this technique is only valid for a low-density fluid such as air, but not for a high-density fluid. Here we will show that the wavelet method works very well for this case by re-computing the examples studied in Mei (2005) — iron rods of circular cross-section embedded in water. The material parameters are $\rho_{iron} = 7670\text{kg/m}^3$, $\rho_{water} = 1000\text{kg/m}^3$, $c_{l,iron} = 6010\text{m/s}$, $c_{l,water} = 1490\text{m/s}$ and $c_{t,iron} = 3230\text{m/s}$; and the filling fraction $f = 0.4$. The band structures are illustrated in Fig. 8. The left part of the figure shows the results for the triangular lattice with iron rods which are accordant with Fig. 3d of Mei (2005); the middle part shows the dispersion relations for the square lattice with iron rods which is identical to Fig. 3c of Mei (2005). The right part corresponds to the inverted structure of the middle part, i.e., a system of the iron host with holes filled by water for which the PWE method fails. In calculation, we take 1024 basis functions.

To check the convergence of the algorithm with the number of the basis functions, we compute the percentage change between the eigenvalues of the longitudinal

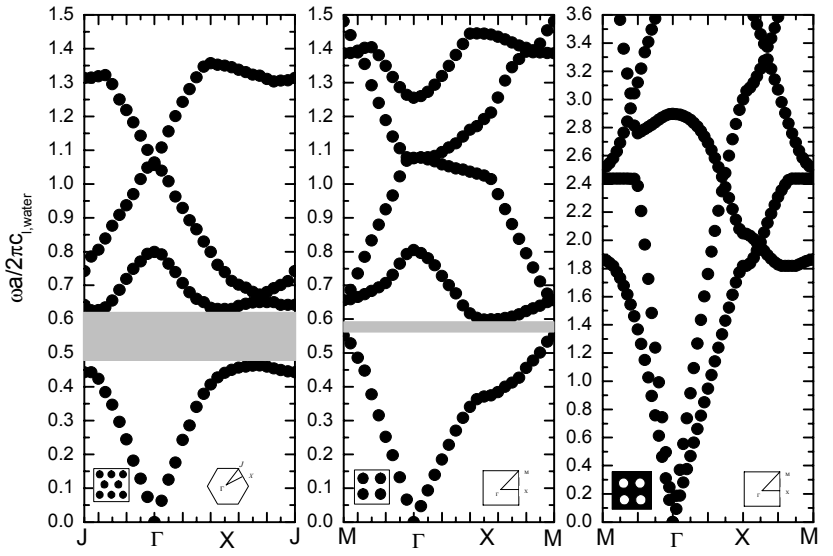

Figure 8: Band structures for iron-water systems: the left is for triangular lattice with iron rods, the middle for square lattice with iron rods, and the right for square lattice with water cylinders

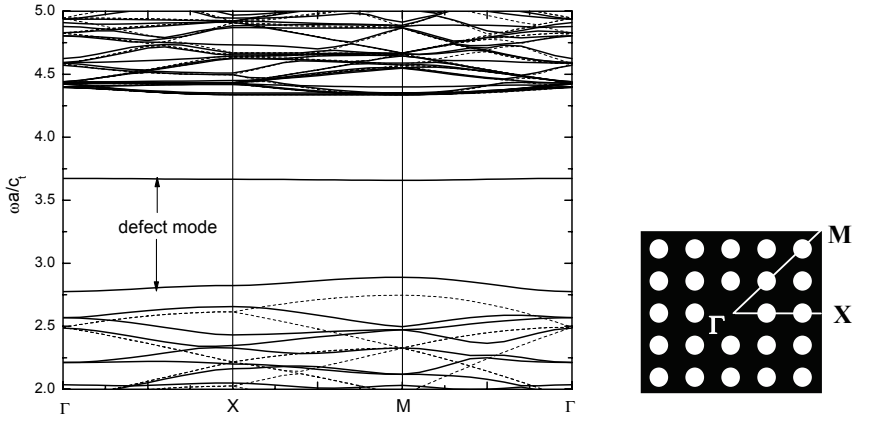

Figure 9: Band structures of transverse modes for an array of vacuum holes in the silicon host with a point defect in a 5×5 supercell, the filling fraction $f = 0.6$

modes obtained by using different basis sizes for the middle and right parts of Fig. 8. The results are listed in Table 2 where the "Maximum % change" and "Average

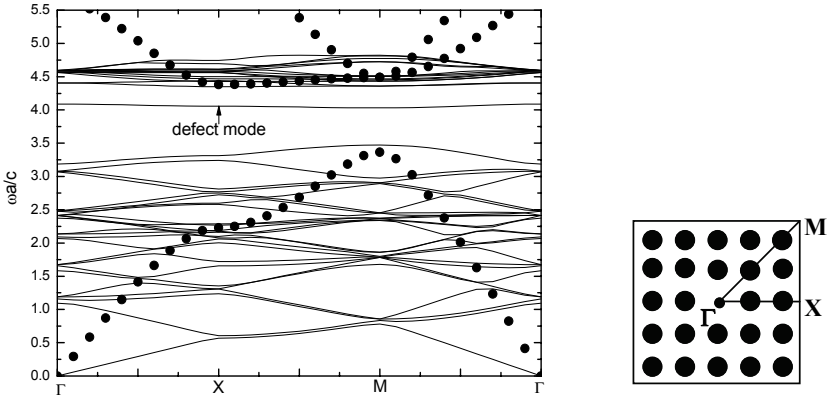

Figure 10: Band structures for an array of steel cylinders in the water host with a point defect in a 5×5 supercell, the filling fraction $f = 0.55$ and $r_d = 0.5r_0$

% change" are defined as

$$\frac{1}{N} \max \left| \omega_{k,N,small\ set} - \omega_{k,N,large\ set} \right|$$

and

$$\frac{1}{N} \left\{ \frac{1}{M} \left| \omega_{k,N,small\ set} - \omega_{k,N,large\ set} \right| \right\}$$

respectively, in which N is the total number of the bands we consider and M is the total number of the points we calculate along one edge of the Brillouin zone, say $\Gamma - X$. Here we take N=4 and M=11. It is shown that 1024 basis functions may yield results with satisfied accuracy.

Table 2: Algorithm's convergence data

	Water host with iron rods		Iron host with water cylinders	
	Maximum % change	Average % change	Maximum % change	Average % change
16 and 256	12.6	5.5	15.89	7.6
256 and 1024	2.1	1.1	5.7	3.54
1024 and 4096	0.5	0.1	1.1	0.68

Next we compute the band structures for systems with defects. The supercell technique, which has been proved very efficient in studying the defect modes of

phononic crystals (Khelif et al. 2003), will be used. We first consider a square lattice of vacuum holes in silicon host with a point defect which is created by filling a hole with silicon. The material parameters of silicon are $\rho_{si} = 2330\text{kg/m}^3$ and $c_{t,si} = 5362\text{m/s}$, the filling fraction $f = 0.6$. The band structures of purely transverse waves are illustrated in Fig. 9 where the solid lines show the results for the system with defects and the dashed lines for the perfect system. Two defect modes are found to appear in the band gaps. The upper one is very flat which implies the localization of the waves in the system. In calculation, we use the 5×5 supercell containing a point defect in the center (see the right part of Fig. 9). To get good accuracy, 4096 basis functions are used in the wavelet expansions. The results are in good agreement with those obtained by Huang and Wu (2005) with the PWE method for the same system (see Fig. 1 in Huang and Wu 2005).

As the second example, we re-compute the system consisting of steel cylinders arranged in water in square lattice with the filling friction $f = 0.55$ which was studied in Wu and Liu (2002) by using the PWE method. We replace a steel cylinder by a smaller one ($r_d = 0.5r_0$) to create a point defect. Again 5×5 supercell and 4096 basis functions are used in calculation. Band structures are shown in Fig. 10 where the dots are results obtained for a perfect system by using the unit cell. A flat defect mode is observed. The results are found in good agreement with those in Wu and Liu 2002 (see Fig. 4 therein).

4.3 Fluid-fluid supercell systems

The fluid-fluid systems are relatively simple because only the longitudinal wave mode is involved. Therefore we will consider systems with defects. As the first example, a square lattice of mercury cylinders in water host with a point defect is computed by using 5×5 supercells, see the right part of Fig. 11. The filling fraction $f = 0.65$ and the filling fraction of defects $f_d = 0.01$. The material parameters of mercury are $\rho_{Hg} = 13500\text{kg / m}^3$ and $c_{l,Hg} = 1450\text{m / s}$. The left part of Fig. 11 illustrates the band structures where a localization mode induced by the defects is observed. The results agree perfectly with Fig. 4-10 in Wu (2001). The convergence of the method for this example is shown in Fig. 12. In calculation, we take 4096 wavelet basis functions. The second example is a square lattice of water cylinders in mercury host with a line defect as shown in the right part of Fig. 13. The filling fraction is $f = 0.3$. The line defect is created by replacing an array of water cylinders with smaller ones ($r_d = 0.5r_0$). The band structures are plotted in Fig. 13 which shows very good agreement with Fig. 4-3 of Wu (2001).

The last four examples (Figs. 9 to 13) show that the wavelet method, together with the supercell technique, is efficient for analysis of the defect states of phononic crystals, although more basis functions are necessary in wavelet expansions be-

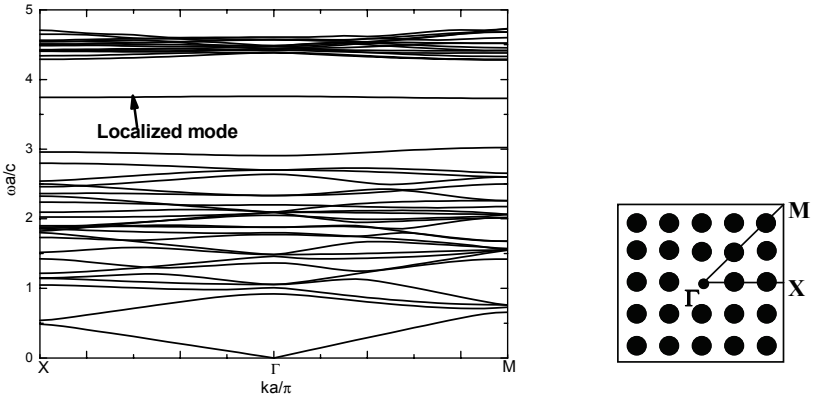

Figure 11: Band structures for an array of mercury cylinders in the water host with a point defect in a 5×5 supercell, the filling fraction $f = 0.65$ and the defect filling fraction $f = 0.01$

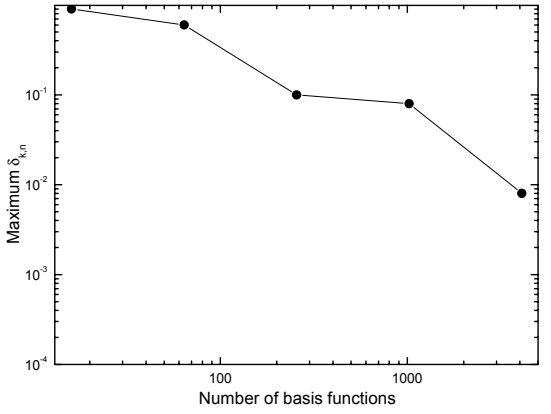

Figure 12: Convergence of the wavelet method: maximum relative error versus the number of wavelet basis functions

cause of large supercell size (generally 5×5).

5 Conclusions

A wavelet-based method is developed in this paper for band structure calculations of two-dimensional phononic crystals. Various numerical examples show some merits of the method. For instance, the method can treat systems with general anisotropic materials. The algorithm converges fast and can yield accurate results

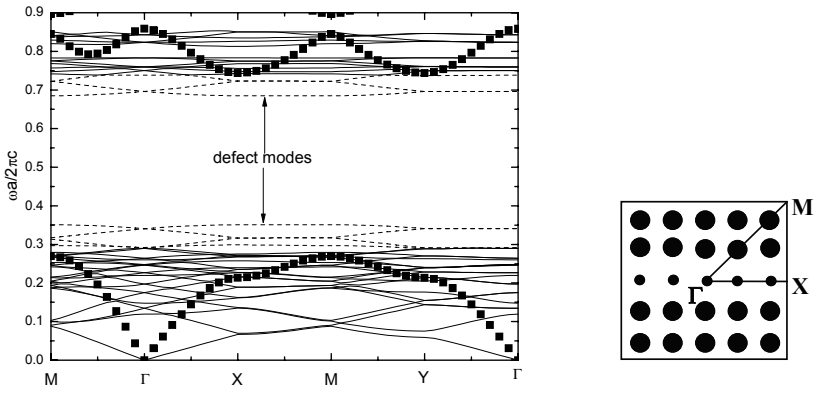

Figure 13: Band structures for an array of water cylinders in the mercury host with a line defect in a 5×5 supercell, the filling fraction $f = 0.3$ and $r_d = 0.5r_0$

with fewer (generally 1024) wavelet basis functions for various lattice structures. The method works efficiently for all kinds of material combinations, including mixed solid-fluid system where the PWE method encounters difficulties. The supercell technique of the wavelet method is also proved efficient although more basis functions are necessary. Generally speaking, the developed wavelet method is expected to be an efficient method in computing the band structures of phononic crystals.

Acknowledgement: The authors gratefully acknowledge support by the National Natural Science Foundation of China under Grant No. 10632020 and the German Research Foundation (DFG) under Grant No. ZH 15/11-1. The last two authors are also grateful to the support by the China Scholarship Council and the German Academic Exchange Service under Grant No. D/08/01795.

References

Ashcroft, N.W.; Mermin, N.D. (1976): *Solid State Physics*. Holt, Rinehart & Winston, New York/London.

Bayindir, M.; Temelkuran, B.; Ozbay, E. (2000): Tight-binding description of the coupled defect modes in three-dimensional photonic crystals. *Physical Review Letters*, vol.84, pp.2140-2143.

Bertoluzza, S.; Canuto, C.; Urban, K. (2000): On the adaptive computation of integrals of wavelets. *Applied Numerical Mathematics*, vol.34, pp.13-38.

Checoury, X.; Lourtioz, J.M. (2006): Wavelet method for computing band diagrams of 2D photonic crystals. *Optics Communications*, vol.259, pp.360-365.

Cohen, A.; Dahmen, W.; Devore, R. (2001): Adaptive wavelet methods for elliptic operator equations: convergence rates. *Mathematics of Computation*, vol.70, pp.27-75.

Cohen, A.; Daubechies, I.; Feauveau, J.C. (1992): Biorthogonal bases of compactly supported wavelets. *Communications in Pure and Applied Mathematics*, vol.45, pp.485-560.

Cohen, A.; Masson, R. (1999): Wavelet methods for second-order elliptic problems, preconditioning, and adaptivity. *SIAM Journal of Science Computation*, vol.21, pp.1006-1026.

Daubechies, I. (1988): Orthogonal bases of compactly supported wavelets. *Communications on Pure and Applied Mathematics*, vol.41, pp.909-996.

David, S.W. (2002): *Fundamentals of Matrix Computations*. John Wiley&Sons, Inc. New York.

Eastham, M.S.P. (1973): *The Spectral Theory of Periodic Differential Equations*. Scottish Academic Press, Edinburgh/London.

Ewing, R.E.; Liu, J.; Wang, H. (2004): Adaptive biorthogonal spline schemes for advection-reaction equations. *Journal of Computational Physics*, vol.193, pp.21-39.

Goffaux, C.; Sa'nchez-Dehesa, J. (2003): Two-dimensional phononic crystals studied using a variational method: Application to lattices of locally resonant materials. *Physical Review B*, vol.67, article no. 144301.

Goffaux, C.; Vigneron, J.P. (2001): Theoretical study of a tunable phononic band gap system. *Physical Review B*, vol.64, article no. 075118.

Haar, A. (1910): Zur theorie der orthogonalen funktionen-systeme. *Mathematical Analysis*, vol.69, pp.331-371.

Han, Z.D.; Atluri, S.N. (2004): A Meshless Local Petrov-Galerkin (MLPG) approach for 3-dimensional elasto-dynamics. *CMC: Computers Materials and Continua*, vol.1, pp.129-140.

Hou, Z.L.; Fu, X.J.; Liu, X.Y. (2004): Calculational method to study the transmission properties of phononic crystals. *Physical Review B*, vol.70, article no. 014304.

Hsieh, P.F.; Wu, T.T.; Sun, J.H. (2006): Three-dimensional phononic band gap calculations using the FDTD method and a pc cluster system. *IEEE Transactions on Ultrasonics, Ferroelectrics, and Frequency Control*, vol.53, pp.148-158.

Huang, Z.Z.; Wu, T.T. (2005): Analysis of wave propagation in phonoinc crystals with channel using the plane-wave expansion and supercell techniques. *IEEE Ultrasonics Symposium*, pp.77-80.

Joannopoulos, J.D.; Meade, R.D.; Winn, J.N. (1995): Photonic Crystals: Molding the Flow of Light, Princeton University Press, Princeton.

Kafesaki, M.; Economou, E.N. (1999): Multiple-scattering theory for three-dimensional periodic acoustic composites. *Physical Review B*, vol.60, pp.11993-12001.

Khelif, A.; Djafari-Rouhani, B.; Vasseur, J.O.; Deymier P.A. (2003): Transmission and dispersion relations of perfect and defect-containing waveguide structures in phononic band gap materials. *Physical Review B*, vol.68, article no. 024302.

Kushwaha, M.S. (1999): Band gap engineering in phononic crystals. *Recent Research Developments in Applied Physics*, vol.2, pp.743-855.

Li, C.; Han, X.; Wen, X. (2006): Band-structure results for elastic waves interpreted with multiple-scattering theory. *Physical Review B*, vol.74, article no. 153101.

Li, X.L.; Wu, F.; Hu, H.; Zhong, S.; Liu, Y.Y. (2003): Large acoustic band gaps created by rotating square rods in two-dimensional periodic composites. *Journal of Physics, D: Applied Physics*, vol.36, pp. L15-L17.

Mallat, S. (1989): Multiresolution and wavelet orthonormal bases in $L^2(R)$. *Transactions of American Mathematical Society*, vol.315, pp.69-87.

Mallat, S. (1999): *A Wavelet tour of signal processing*, second ed. Academic Press, San Diego.

Meyer, Y. (1992): *Wavelets and operators I*. Cambridge University Press, Cambridge.

Mei, J. (2005): *Research on acoustic or elastic wave band gaps of phononic crystals*. Master's thesis, Wuhan University, China (in Chinese).

Mitra, M.; Gopalakrishnan, S. (2006): Wavelet based 2-D spectral finite element formulation for wave propagation analysis in isotropic plates. *CMES: Computer Modeling in Engineering and Science*, vol.15, pp.49-68.

Niklasson, A.M.N.; Tymczak, C.J.; Roder, H. (2002): Multiresolution density-matrix approach to electronic structure calculations. *Physical Review B*, vol.66, article no. 155120.

User, M. (1996): Approximation power of biorthogonal wavelet expansions. *IEEE Transactions of Signal Processing*, vol.44, pp.519-527.

User, M.; Blu, T. (1998): Comparison of wavelets from the point of view of their approximation error. In: Wavelet applications in signal and imaging processing VI,

Proceedings of SPIE, vol.3458, pp.14-21.

Sainidou, R.; Stefanou, N.; Modinos, A. (2004): Green's function formalism for phononic crystals. *Physical Review B*, vol.69, article no. 064301.

Santos, J.C.; Cruz, P.; Alves, M.A.; Oliveira, P.J.; Magalhaes, F.D.; Mendes, A. (2004): Adaptive multiresolution approach for two-dimensional PDEs. *Computer Methods in Applied Mechanics and Engineering*, vol.193, pp.405-425.

Sigalas, M.M.; Garcia, N. (2000): Theoretical study of three dimensional elastic band gaps with the finite-difference time-domain method. *Journal of Applied Physics*, vol.87, pp. 3122-3125.

Tanaka, Y.; Tamura, S.I. (1998): Surface acoustic waves in two-dmensional periodic elastic structures. *Physical Review B*, vol.58, pp.7958-7965.

Wang, G.; Wen, J.H.; Han, X.Y.; Zhao, H.G. (2003): Finite difference time domain method for the study of band gap in two-dimensional phononic crystals. *Acta Physica Sinica*, vol.52, pp.1943-1947 (in Chinese).

Wang, G.; Wen, J.H.; Liu, Y.Z.; Wen, X. (2004): Lumped-mass method for the study for band structure in two-dimensional phononic crystals. *Physical Review B*, vol.69, article no. 184302.

Wu, F.G.; Liu, Y.Y. (2002): Acousitc band gaps and defect states in two dimensional composite materials. *Acta Physica Sinica*, vol.51, pp.1434-1438 (in Chinese).

Wu, F.G. (2001): *Research on band gaps and defect modes in phononic crystals*. Doctor's thesis, South China University of Technology, China (in Chinese).

Xiang, J.W, Chen, X.; Feng, Y; Fianfa, Y.; Zheng, J. (2008): A class of wavelet-based flat shell elements using B-spline wavelet on the interval and its applications. *CMES: Computer Modeling in Engineering and Science*, vol.23, pp.1-12.

Yablonovitch, E.; Gmitter, T.J.; Meade, R.D.; Rappe, A.M.; Brommer K.D.; Joannopoulos, J.D. (1991): Donor and acceptor modes in photonic band-structure. *Physical Review Letters*. vol.67, pp.3380-3383.

Zhang, J. (2007): A comparative study of non-separable wavelet and tensor-product wavelet in image compression. *CMES: Computer Modeling in Engineering and Science*, vol.22, pp. 91-96.

Zhang, S.; Hua, J.; Cheng, J.C. (2003): Experimental and theoretical evidence for the existence of broad forbidden gaps in the three-component composite. *Chinese Physics Letter*, vol.20, pp.1303-1305.